IEEE Access
Multidisciplinary ⋮ Rapid Review ⋮ Open Access Journal

Received 25 October 2023, accepted 30 October 2023, date of publication 8 November 2023, date of current version 16 November 2023.

Digital Object Identifier 10.1109/ACCESS.2023.3331107

RESEARCH ARTICLE

Harmonic Balance Design of Oscillatory Circuits Based on Stanford Memristor Model

MAURO DI MARCO[1], MAURO FORTI[1], GIACOMO INNOCENTI[2], AND ALBERTO TESI[2]
[1]Department of Information Engineering and Mathematics, University of Siena, 53100 Siena, Italy
[2]Department of Information Engineering, University of Florence, 50139 Firenze, Italy

Corresponding author: Mauro Di Marco (mauro.dimarco@unisi.it)

This work was supported in part by the Analogue COmputing with Dynamic Switching Memristor Oscillators: Theory, Devices and Applications (COSMO), under Grant PRIN 2017LSCR4K 002, and in part by the Italian Ministry of Education, University and Research (MIUR).

ABSTRACT Oscillatory circuits with real memristors have attracted a lot of interest in recent years. The vast majority of circuits involve volatile memristors, while less explored is the use of non-volatile ones. This paper considers a circuit composed by the interconnection of a two-terminal (one port) element, based on the linear part of Chua's circuit, and a non-volatile memristor obeying the Stanford model. A peculiar feature of such a memristor is that its state displays negligible time-variations under some voltage threshold. Exploiting this feature, the memristor is modeled below threshold as a programmable nonlinear resistor whose resistance depends on the gap distance. Then, the first-order Harmonic Balance (HB) method is employed to derive a procedure to select the parameters of the two-terminal element in order to generate programmable subthreshold oscillatory behaviors, within a given range of the gap, via a supercritical Hopf bifurcation. Finally, the dynamic behaviors of the designed circuits as well as the sensitivity of the procedure with respect to the location of the bifurcating equilibrium point and the range of the gap are discussed and illustrated via some application examples.

INDEX TERMS Bifurcations, Chua's circuit, harmonic balance, memristor, stanford model.

I. INTRODUCTION

Recent years have shown an ever growing interest in developing in-memory computing schemes to tackle some problems emerging in digital Von Neumann systems [1], [2], [3]. Among others nanoscale devices, circuits with memristors appear to be a promising tool for implementing new in-memory, analog and parallel (neuromorphic) computing paradigms [4], [5], [6], [7], [8].

The theory underlying the dynamics of circuits with ideal memristors is nowadays quite mature (see [9] and references therein). One main limitation of ideal memristors is that they are unable to accurately model the switching dynamics of real memristor devices implemented in nanotechnology. On the other hand, real memristors are usually modeled via the so called generic or extended memristor models, that usually involve general forms of quasi static Ohm's law and also extended forms for the state variable equations. Real memristors can be non-volatile, as it happens in the ideal case, but also volatile, a typical example being the thermistor. Moreover, different from ideal memristors, the real ones usually feature a voltage threshold such that the state has almost negligible variations below threshold, while they display rapid big variations beyond threshold.

Several oscillatory circuits based on the negative differential resistance (NDR) displayed by the quasi-static nonlinear characteristic of volatile memristors have been considered in the technical literature [10], [11], [12], [13], [14], [15], [16]. Their operating principle is akin to that of the Anson-Pearson electronic oscillators. A less explored and less obvious possibility is to built up oscillators using non-volatile memristors [17], [18]. An interesting related question concerns the possibility to take advantage in view of the applications of the programmability features of non-volatile memristor devices.

Recently, it has been shown that modeling non-volatile memristors as programmable nonlinear resistors can be fruitfully exploited for the design of oscillatory circuits given by the interconnection of the memristor with a

The associate editor coordinating the review of this manuscript and approving it for publication was Artur Antonyan.

two-terminal linear element [19], [20]. A Chua's oscillatory circuit with a non-volatile extended memristor obeying Stanford model is designed in [19], showing via numerical simulations that it is capable to generate quite different coexisting dynamics. In [20] an oscillatory Chua's circuit based on a non-volatile memristive device is realized and its rich dynamic behavior is validated experimentally. In both contributions the design procedure relies on the observation that the memristor state variable (the gap distance in [19]) has almost negligible variations when its voltage is below some threshold. This permits to model the memristor as a nonlinear resistor whose resistance can be programmed for instance by applying voltage pulses above the threshold. The parameters of the two-terminal element are selected by satisfying some conditions ensuring desired stability properties of the equilibriun points of the memristor circuit.

This paper considers the same circuit of [19], i.e., a non-volatile extended memristor obeying Stanford model connected to a two-terminal (one port) linear time-invariant element given by the parallel interconnection of the classic Chua's circuit and a linear resistor with negative conductance. The goal is to develop a systematic procedure to design the parameters of the two-terminal element in order to ensure that some given equilibrium point of the circuit undergoes a supercritical Hopf bifurcation at some given value of the gap distance, thus generating a family of (stable) periodic solutions within some range of the gap. The procedure is based on the first-order Harmonic Balance (HB) method, a well-known technique for predicting limit cycles and their bifurcations as well as more complex behaviors (see [21] and references therein). The first order HB method is applied to the third-order circuit obtained by replacing the non-volatile extended memristor obeying Stanford model with a nonlinear resistor whose resistance depends on the gap distance, which is assumed to be constant when the voltage is below some given threshold. This is discussed in Section II together with the problem formulation and a brief summary of the HB method. The application of the HB method permits to identify the set of the parameters of the two-terminal element ensuring the occurrence of a supercritical Hopf bifurcation. This is shown in Section III where for each value of the gap a first-order Predicted Limit Cycle (PLC) approximating the corresponding periodic solution of the family generated by the bifurcation is determined, also providing a quantitative measure of their distance. Based on these results, in Section IV a systematic procedure is derived for selecting the parameters of the two-terminal element guaranteeing that the PLCs are close to the stable periodic solutions generated by the Hopf bifurcation within some given range of the gap. The dynamic behaviors displayed by the designed two-terminal element coupled with both the programmable nonlinear resistor and the non-volatile extended memristor obeying Stanford model are discussed, together with the sensitivity of the procedure with respect to the location of the equilibrium point and the value of the gap distance at which the Hopf bifurcation occurs. Some final conclusions end the paper in Section V.

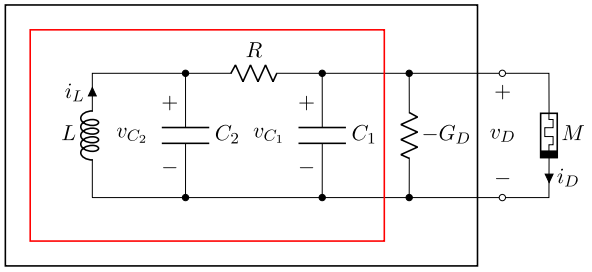

FIGURE 1. Two-terminal element (black box), memristor (*M*) and linear part of the classic Chua's circuit (red box).

II. MEMRISTOR CHUA'S CIRCUIT AND PROBLEM FORMULATION

In this paper we consider the circuit of Fig. 1 where a two-terminal (one port) linear time-invariant element is interconnected to a memristor. The two-terminal linear element is composed by a linear resistor ($R > 0$), two capacitors ($C_1 > 0$, $C_2 > 0$), an inductor ($L > 0$), and a linear resistor with a negative conductance $-G_D$ ($G_D > 0$). Other topologies, employing an active memristor, can be adopted and are available in the literature [22]. It is worth noting that the circuit has the same structure of the celebrated Chua's circuit where the nonlinear resistor is replaced by the parallel interconnection of the memristor with the linear resistor with negative conductance. It is assumed that the memristor is described by the Stanford model of RRAM devices [23], [24], [25], [26]. The relation between the current i_D and the voltage v_D has the following expression

$$i_D = I_0 \exp\left(-\frac{g}{g_0}\right) \sinh\left(\frac{v_D}{V_0}\right), \tag{1}$$

where g is the gap distance, which is defined as the average distance between the top electrode and the tip of the (dominant) conductive filament, and I_0, V_0, g_0 are constant parameters whose values are reported in Table 1. The gap distance g represents the internal state variable of the memristor and it has a lower limit $g_{\min}$ and an upper limit $g_{\max}$, respectively, i.e., $g \in [g_{\min}, g_{\max}]$. Specifically, $g_{\min}$ is reached when the tip of the conductive filament is nearly in contact with the top electrode during the SET process, i.e., the switching from the high-resistance state (HRS) to the low-resistance state (LRS), while $g_{\max}$ is the residual conductive filament during the RESET process, i.e., the switching from LRS to HRS. The values of $g_{\min}$ and $g_{\max}$ are reported in Table 1.

TABLE 1. Stanford model parameters.

Symbol	Unit	Value	Description
I_0	A	6.14×10^{-5}	$i - v$ fitting parameter
V_0	V	0.43	=
g_0	m	2.75×10^{-10}	=
$g_{\min}$	m	0.1×10^{-9}	Minimum gap distance
$g_{\max}$	m	1.7×10^{-9}	Maximum gap distance

The Stanford model is completely described by (1) and the following two differential equations

$$\frac{dg}{dt} = -v_0 \left(\exp\left(-\frac{qE_{\text{ag}}}{kT}\right) \exp\left(\frac{qa_0\gamma}{\ell kT} v_D\right) - \exp\left(-\frac{qE_{\text{ar}}}{kT}\right) \exp\left(-\frac{qa_0\gamma}{\ell kT} v_D\right)\right) \tag{2}$$

$$\frac{dT}{dt} = \frac{v_D i_D}{C_{\text{th}}} - \frac{T - T_0}{R_{\text{th}} C_{\text{th}}} \tag{3}$$

where T is the temperature, v_0, q, k, a_0, ℓ, E_{ag}, E_{ar}, C_{th}, R_{th}, T_0 are given constants (see, e.g., [19]), and γ is a g-dependent local field enhancement factor, given by

$$\gamma = \gamma_0 - \beta \left(\frac{g}{g_1}\right)^3,$$

with γ_0, β and g_1 being fitting parameters obtained from experimental current-voltage curves [19].

The dynamics of the circuit of Fig. 1 has been thoroughly investigated in [19] for some given values of R, C_1, C_2, L, and G_D. Notably, it has been shown that the gap g remains practically constant over time if v_D satisfies

$$|v_D(t)| \leq V_T, \tag{4}$$

where V_T is some given voltage threshold. As a consequence, the memristor simply works as a programmable nonlinear resistor, whose voltage-current characteristic (1) can be written as

$$i_D(v_D; \mu) := I_0 \exp(-\mu) \sinh\left(\frac{v_D}{V_0}\right), \quad \mu \in I_\mu, \tag{5}$$

where $\mu := \dfrac{g}{g_0}$ is the normalized gap distance and

$$I_\mu := \left[\frac{g_{\min}}{g_0}, \frac{g_{\max}}{g_0}\right] = [0.26, 6.18]. \tag{6}$$

This paper deals with the problem of designing R, C_1, C_2, L, and G_D in order that the circuit of Fig. 1, once the memristor is modeled by the programmable nonlinear resistor described by (5), displays desired oscillatory behaviors for given values of the programmable parameter μ. It is expected that if the constraint (4) holds then these oscillations are also exhibited when the complete memristor model (1)-(3) is used in place of (1), i.e., (5).

The remainder of this Section is organized as follows. In Section II-A, it is shown that the circuit can be cast as the input-output feedback system of Fig. 2, which is usually referred to as Lur'e system. Lur'e systems have received a lot of attention in the literature (see [27] and references therein), since their structure emerges in several control problems and it is enjoyed by many oscillatory circuits (e.g., Duffing, Van der Pol). In Section II-B, we recall the main elements of the general Harmonic Balance (HB) method which is a key tool for the prediction of limit cycles and their bifurcations as well as more complex behaviors (see [21] and references therein), while Section II-C focuses on the first-order HB method which is usually known as the Describing Function (DF) technique. Finally, the problem of interest is formulated in Section II-D.

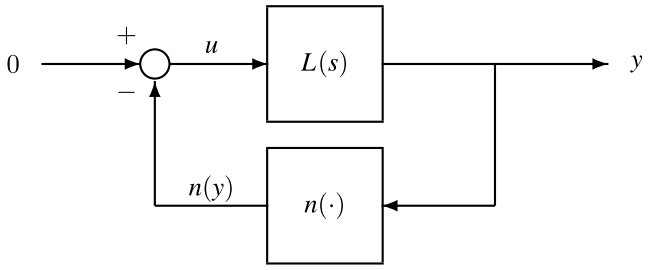

FIGURE 2. Lur'e system: $L(s)$ is the transfer function of the linear system in the forward path and $n(\cdot)$ is the memoryless nonlinear characteristic of the feedback path.

A. LUR'E SYSTEM REPRESENTATION OF THE MEMRISTOR CIRCUIT

Under the assumption that the gap distance is constant, the dynamics of the circuit of Fig. 1 obeys the following equations

$$\begin{cases} C_1 \dot{v}_{C_1}(t) &= \dfrac{1}{R}\left(v_{C_2}(t) - v_{C_1}(t)\right) + G_D v_{C_1}(t) - i_D(t) \\ C_2 \dot{v}_{C_2}(t) &= \dfrac{1}{R}\left(v_{C_1}(t) - v_{C_2}(t)\right) + i_L(t) \\ L \dot{i}_L(t) &= -v_{C_2}(t), \end{cases} \tag{7}$$

where v_{C_1} and v_{C_2} are the capacitor voltages, i_L is the inductor current, and i_D depends on v_D and μ according to (5)-(6). By introducing the state vector $x = (x_1, x_2, x_3)^\top$ with $x_1 = v_{C_1}$, $x_2 = v_{C_2}$, $x_3 = i_L$ and observing that $v_D = v_{C_1}$, we can rewrite (7) in the following state space form

$$\begin{cases} \dot{x}(t) &= Ax(t) + Bu(t) + Ey(t) \\ y(t) &= Cx(t), \end{cases} \tag{8}$$

where

$$A = \begin{pmatrix} -\dfrac{1}{RC_1} & \dfrac{1}{RC_1} & 0 \\ \dfrac{1}{RC_2} & -\dfrac{1}{RC_2} & \dfrac{1}{C_2} \\ 0 & -\dfrac{1}{L} & 0 \end{pmatrix} \quad B = \begin{pmatrix} \dfrac{1}{C_1} \\ 0 \\ 0 \end{pmatrix} \tag{9}$$

$$C = \begin{pmatrix} 1 & 0 & 0 \end{pmatrix} \quad E = \begin{pmatrix} \dfrac{G_D}{C_1} \\ 0 \\ 0 \end{pmatrix}, \tag{10}$$

$y = v_D$ and

$$u(t) = -i_D(y(t); \mu). \tag{11}$$

It turns out that this state space model can be represented as the Lur'e system of Fig. 2 where $y = x_1 = v_D$, $L(s)$ is the input-ouput transfer function of (8) and

$$n(y) = i_D(y; \mu). \tag{12}$$

It can be verified that $L(s)$ has the following expression

$$L(s) = \frac{\bar{L}(s)}{1 - G_D\bar{L}(s)}, \tag{13}$$

where

$$\begin{aligned}\bar{L}(s) &= C(sI-A)^{-1}B \\ &= \frac{\frac{1}{C_1}\left(s^2 + \frac{1}{RC_2}s + \frac{1}{LC_2}\right)}{s^3 + \frac{1}{R}\left(\frac{1}{C_1} + \frac{1}{C_2}\right)s^2 + \frac{1}{LC_2}s + \frac{1}{RLC_1C_2}},\end{aligned} \tag{14}$$

It is worth noting that $L(s)$ represents the impedance of the two-terminal element of the circuit of Fig. 1 and $\bar{L}(s)$ is the impedance of the linear part of the classic Chua's circuit (red box in Fig. 1), while the nonlinear characteristic of the feedback path depends on the normalized gap distance μ. It can be verified that the Lur'e system admits the following equivalent time domain description[1]

$$\left(\bar{P}(\mathcal{D}) - G_D\bar{Q}(\mathcal{D})\right) y(t) + \bar{Q}(\mathcal{D})n(y(t)) = 0, \tag{15}$$

where $\bar{Q}(\mathcal{D})$ and $\bar{P}(\mathcal{D})$ are the numerator and denominator polynomials of $\bar{L}(\mathcal{D})$, respectively. Summing up, under the assumption that the gap g is constant, the circuit of Fig. 1 can be represented as a one-parameter family of Lur'e systems indexed by μ whose dynamics is governed by third-order differential equations.

B. THE HARMONIC BALANCE (HB) METHOD

In the HB method the steady-state periodic output of period $T > 0$ of the forward path of the Lur'e system of Fig. 2 and the corresponding T-periodic output of the feedback path are first expressed as

$$\bar{y}(t) = \sum_{k=-\infty}^{+\infty} \gamma_k e^{jk\omega t} \tag{16}$$

and

$$n(\bar{y}(t)) = \sum_{k=-\infty}^{+\infty} \delta_k e^{jk\omega t}, \tag{17}$$

respectively, where $\omega := 2\pi/T$ and

$$\gamma_k = \frac{\omega}{2\pi}\int_{-\pi/\omega}^{\pi/\omega} \bar{y}(t)e^{-jk\omega t}dt, \quad \gamma_{-k} = \gamma_k^*, \quad k = 0, 1, \ldots \tag{18}$$

$$\delta_k = \frac{\omega}{2\pi}\int_{-\pi/\omega}^{\pi/\omega} n(\bar{y}(t))e^{-jk\omega t}dt, \quad \delta_{-k} = \delta_k^*, \quad k = 0, 1, \ldots, \tag{19}$$

with * denoting the conjugate operator. Then, the steady-state T-periodic output of the linear system in the forward path generated by the input $-n(\bar{y}(t))$, which is given by

$$\tilde{y}(t) = \sum_{k=-\infty}^{+\infty} L(j\omega)\delta_k e^{jk\omega t}, \tag{20}$$

is equated to $\bar{y}(t)$ in (16) leading to the HB equations

$$\gamma_k + L(jk\omega)\delta_k = 0, \quad k = 0, 1, \ldots, \tag{21}$$

where each coefficient δ_k depends on γ_h, $h = 0, 1, \ldots$, according to (19). The HB equations are usually solved in an approximate way by considering for both $\bar{y}(t)$ and $n(\bar{y}(t))$ a finite number of harmonic terms. Specifically, the N-th order Predicted Limit Cycle (PLC) of the Lur'e system of Fig. 2 is defined as

$$\bar{y}_N(t) = \sum_{k=-N}^{N} \gamma_k e^{jk\omega t} \tag{22}$$

where ω and γ_k, $k = 0, 1, \ldots, N$ solve the N-th order HB equations

$$\gamma_k + L(jk\omega)\delta_k(\gamma_0, \gamma_1, \ldots, \gamma_N) = 0, \quad k = 0, 1, \ldots, N, \tag{23}$$

with $\delta_k(\gamma_0, \gamma_1, \ldots, \gamma_N)$, $k = 0, 1, \ldots, N$, computed according to (19) once $\bar{y}(t)$ is replaced by $\bar{y}_N(t)$. Clearly, N-th order PLCs are only approximations of true limit cycles. Indeed, the existence of a true limit cycle nearby the PLC can be rigorously proven if restrictions are placed on the feedback interconnection even in the case $N = 1$ (see, e.g., [27], [28]). These conditions basically quantify the so-called filtering hypothesis, i.e., the gains $|L(jk\omega)|$, $k = N + 1, \ldots$, of the linear system in the forward path and the higher order coefficients δ_k, $k = N + 1, \ldots$ generated by the nonlinearity in the feedback path are negligible. This follows from the fact that, since $\bar{y}_N(t)$ solves the N-th order HB equations, $\tilde{y}(t)$ boils down to

$$\tilde{y}(t) = \bar{y}_N(t) + \sum_{k=-N-1}^{N+1} L(jk\omega)\delta_k e^{jk\omega t}. \tag{24}$$

A quantitative measure of the filtering hypothesis is the so-called distortion index (see, e.g., [29]), which can be

[1] $\mathcal{D}$ denotes the time-differential operator (i.e., $\mathcal{D}y(t) = \dot{y}(t)$, $\mathcal{D}^2y(t) = \ddot{y}(t)$ and so on).

expressed as

$$D_N(\gamma_0, \ldots, \gamma_N, \omega) = \frac{\|\tilde{y}(t)) - \bar{y}_N(t)\|_2}{\|y_0(t)\|_2} = \sqrt{\frac{2\sum_{k=N+1}^{+\infty} |L(jk\omega)|^2 \delta_k^2(\gamma_0, \ldots, \gamma_N)}{\gamma_0^2 + 2\sum_{k=1}^{N} \gamma_k^2}}, \quad (25)$$

where $\|\cdot\|_2$ denotes the L_2-norm on the period T. Clearly, in the limiting case $D_N(\gamma_0, \ldots, \gamma_N, \omega) = 0$, i.e, $\tilde{y}(t) = \bar{y}_N(t)$, the PLC is indeed a true limit cycle.

C. THE FIRST-ORDER HB METHOD

In the first-order HB method the PLC is expressed as

$$\bar{y}_1(t) = A + B\cos\omega t, \quad (26)$$

where A is the bias term and $B > 0$ is the amplitude of the harmonic term. Since $\gamma_0 = A$ and $\gamma_1 = B/2$, it turns out that any first-order PLC is obtained by solving with respect to A, $B > 0$, and $\omega > 0$ the following first-order HB equations:

$$A + L(0)N_0(A, B)A = 0, \quad (27)$$
$$1 + L(j\omega)N_1(A, B) = 0, \quad (28)$$

where

$$N_0(A, B) = \frac{1}{2\pi A}\int_{-\pi}^{\pi} n(A + B\cos\theta)\, d\,\theta, \quad (29)$$

and

$$N_1(A, B) = \frac{1}{\pi B}\int_{-\pi}^{\pi} n(A + B\cos\theta)\, e^{-j\theta}\, d\,\theta \quad (30)$$

are known as the (dual-input) Describing Functions (DFs) of the nonlinearity $n(\cdot)$ [30]. Accordingly, the distortion index (25) becomes[2]

$$D_1(A, B, \omega) = 2\sqrt{\frac{\sum_{k=2}^{+\infty} |L(jk\omega)|^2 \delta_k^2(A, B)}{2A^2 + B^2}}. \quad (31)$$

It can be verified that for sufficiently smooth functions $n(\cdot)$ the DFs in the limiting case $B = 0$ boil down to

$$N_0(A, 0)A = n(A)$$
$$N_1(A, 0) = n'(A), \quad (32)$$

with $n'(y)$ denoting the first derivative of $n(y)$, while the distortion index (31) vanishes, i.e.

$$D_1(A, 0, \omega) = 0. \quad (33)$$

The 0-order PLC is a constant signal

$$\bar{y}_0(t) = y_E, \quad (34)$$

which is referred to as an output equilibrium point (OEP) of the Lur'e system of Fig. 2 and it solves the following HB equation:

$$y_E + L(0)n(y_E) = 0. \quad (35)$$

Note that OEPs of Lur'e systems are the constant solutions of the differential equation governing the system dynamics (eq. (15) in our case).

The first-order HB method has been employed also to investigate bifurcations of limit cycles in Lur'e systems (see, e.g., [31]). In particular, *Hopf bifurcations* are characterized by the solutions $A = A_H$, $B = 0$ and $\omega = \omega_H$ of (27)-(28) which, exploiting relations (32), reduce to

$$\begin{cases} A_H + L(0)n(A_H) = 0 \\ 1 + L(j\omega_H)n'(A_H) = 0. \end{cases} \quad (36)$$

Note that the first equality implies that the system has an OEP at $y_E = A_H$, while the second one ensures that the rational transfer function $1 + L(s)n'(A_H)$ has two zeroes at $s = \pm j\omega_H$. If all remaining zeros have negative real part, then it is possible to conclude that the equilibrium point at $y_E = A_H$ undergoes a Hopf bifurcation as some parameter of the Lur'e system is varied. One way to assess the stability character of the bifurcation resorts to investigate how the solution of the HB equations for small values of B induced by such a parameter variation is related to the change of the stability properties of the bifurcating equilibrium point [32]. Specifically, if for small B the first-order PLC coexists with a (locally) asymptotically stable (resp. unstable) OEP, then the Hopf bifurcation is subcritical (resp. supecritical).

Period-doubling bifurcations of limit cycles have been investigated by modeling the emerging $2T$-periodic output of Lur'e systems as

$$\bar{y}_2(t; \nu) = A + B\cos\omega t + \nu\cos\left(\frac{\omega}{2}t + \varphi\right), \quad (37)$$

where ν is a small positive coefficient and $\varphi \in [0, 2\pi)$ [33]. Specifically, a *Predicted Period-Doubling* bifurcation (PPD) is said to occur if $\bar{y}_2(t; \nu)$ is indeed a second-order PLC for $\nu \to 0$. This requires to derive the second-order HB equations, taking into account that $\omega/2$ is now that basic frequency, and then considering the limiting case $\nu = 0$. It can be shown (see, e.g., [33]) that the PLC (26) undergoes a (first) PPD bifurcation as some parameter of the Lur'e system is varied, if A, B, and ω solve the first-order HB equations (27)-(28) plus the following algebraic equation:

$$\left|L^{-1}\left(j\frac{\omega}{2}\right) + F_0(A, B)\right| = |F_1(A, B)|, \quad (38)$$

where

$$F_0(A, B) = \frac{1}{2\pi}\int_{-\pi}^{\pi} n'(A + B\cos\theta)\, d\theta \quad (39)$$

$$F_1(A, B) = \frac{1}{2\pi}\int_{-\pi}^{\pi} n'(A + B\cos\theta)e^{-j\theta}\, d\theta. \quad (40)$$

[2] In practice, the distortion index is approximately computed by assuming that $|L(jk\omega)||\delta_k| = 0$ for $k \geq K_h$. Indeed, there are nonlinearities (e.g., polynomials) whose harmonic terms δ_k are exactly equal to zero for k larger than some K_h.

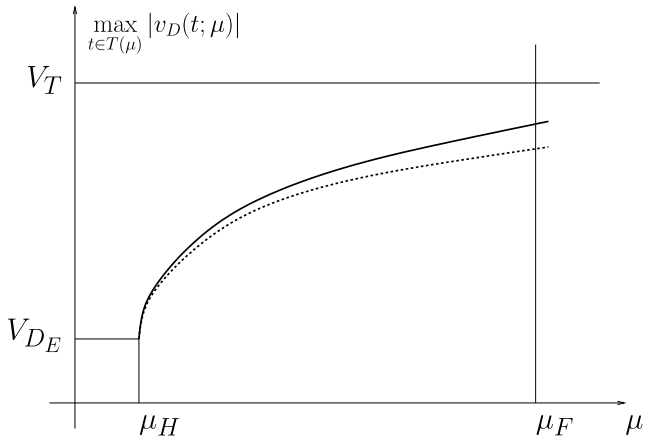

FIGURE 3. Hopf bifurcation: $\max_{t\in T(\mu)} |v_D(t;\mu)|$ (solid curve) and $\max_{t\in T(\mu)} |v_D^0(t;\mu)| = A(\mu) + B(\mu)$ (dashed curve) as a function of μ.

D. PROBLEM FORMULATION

We are interested in selecting the circuit parameters R, C_1, C_2, L, and G_D in order to ensure that the equilibrium point defined by the constant solution $v_D(t) = V_{D_E}$ undergoes a supercritical Hopf bifurcation at $\mu = \mu_H$, $\mu_H \in I_\mu$, which generates a family of (stable) periodic solutions $v_D(t;\mu)$ of period $T(\mu)$. It is also required that the periodic solution emerging from the Hopf bifurcation has a period $T(\mu_H) = 2\pi/\omega_H$ for some given ω_H.

From Section II-A we know that $v_D(t;\mu)$ is the output of the Lur'e system of Fig. 2 and, as outlined in Section II-B, it should satisfy the general HB equations (21). Since solving (21) is quite a difficult problem from a computational viewpoint, we proceed by employing the first-order HB method, thus looking for the PLCs family

$$v_D^0(t;\mu) = A(\mu) + B(\mu)\cos\omega(\mu)t, \quad \mu \in [\mu_H, \mu_F], \tag{41}$$

for some $\mu_F \in I_\mu$. Clearly, $A(\mu_H) = V_{D_E}$, $B(\mu_H) = 0$, $\omega(\mu_H) = \omega_H$, with μ_H, ω_H and V_{D_E} being given positive constants characterizing the Hopf bifurcation.[3] It is worth noting that the constraint (4) boils down to

$$A(\mu) + B(\mu) \le V_T, \quad \mu \in [\mu_H, \mu_F]. \tag{42}$$

Figure 3 provides a sketch of the true and approximated bifurcation diagrams. The former is given by the maximum values of $v_D(t;\mu)$ over the period $T(\mu)$, i.e., $\max_{t\in T(\mu)} |v_D(t;\mu)|$, while the latter by $\max_{t\in T(\mu)} |v_D^0(t;\mu)| = A(\mu) + B(\mu)$. The distance between the two bifurcation diagrams vanishes at $\mu = \mu_H$, since at the Hopf bifurcation $v_D(t;\mu_H) = v_D^0(t;\mu_H) = V_{D_E}$, and it is generally an increasing function of μ. This suggests that it is enough to check the accuracy of the PLC only at $\mu = \mu_F$. Consequently, the circuit parameters R, C_1, C_2, L, and G_D can be selected in order to ensure that the distortion index (31) is sufficiently small at $\mu = \mu_F$.

[3]The assumption $V_{D_E} > 0$ is not restrictive since the odd symmetry of the Lur'e system ensures that the family of PLCs for $V_{D_E} < 0$ is simply obtained by reversing the sign of $A(\mu)$ in (41).

III. PLCS CHARACTERIZATION OF THE MEMRISTOR CHUA'S CIRCUIT

Each PLC of the family (41) must satisfy (27)-(28) where the DFs (29) and (30) are given by

$$N_0(A,B) = \frac{I_0}{V_0}\exp(-\mu)\frac{\sinh\left(\frac{A}{V_0}\right)}{\frac{A}{V_0}}\mathcal{J}_0\left(\frac{B}{V_0}\right) \tag{43}$$

and

$$N_1(A,B) = 2\frac{I_0}{V_0}\exp(-\mu)\cosh\left(\frac{A}{V_0}\right)\frac{\mathcal{J}_1\left(\frac{B}{V_0}\right)}{\frac{B}{V_0}}, \tag{44}$$

with $\mathcal{J}_0(\cdot)$ and $\mathcal{J}_1(\cdot)$ being the modified Bessel function of degree 0 and degree 1 [30].

Since $N_1(A,B)$ is a real function, (28) can be solved only if the frequency $\omega > 0$ of the *PLC* is such that $\mathrm{Im}[L(j\omega)] = 0$, and hence, taking into account (13), only if

$$\mathrm{Im}[\bar{L}(j\omega)] = 0. \tag{45}$$

Note that the possible frequency values of the PLCs are those at which the impedance of the linear part of the classic Chua's circuit is real and they do not vary with the index μ. This implies that the PLCs family (41) satisfies (27)-(28) only if $\mathrm{Im}[\bar{L}(j\omega_H)] = 0$ and

$$\omega(\mu) = \omega_H, \quad \mu \in [\mu_H, \mu_F]. \tag{46}$$

If we set $A_0 := A/V_0$, $B_0 := B/V_0$, and

$$\Gamma_H := \mathrm{Re}[\bar{L}(j\omega_H)], \tag{47}$$

then (27) and (28) can be rewritten as the real equations

$$G_D - \frac{1}{R} = \frac{I_0}{V_0}\exp(-\mu)\frac{\sinh(A_0)}{A_0}\mathcal{J}_0(B_0) \tag{48}$$

and

$$G_D - \frac{1}{\Gamma_H} = \frac{I_0}{V_0}\exp(-\mu)\cosh(A_0)\ 2\frac{\mathcal{J}_1(B_0)}{B_0}, \tag{49}$$

respectively.

Clearly, (27) and (28) admit the PLCs (41) if and only if (46) holds and (48)-(49) are satisfied by $A_0(\mu) = A(\mu)/V_0$ and $B_0(\mu) = B(\mu)/V_0$ for all $\mu \in [\mu_H, \mu_F]$. The next result provides the sought first-order PLCs family (41) generated by the supercritical Hopf bifurcation occurring at $\mu = \mu_H$.

Proposition 1: Let $V_{D_E} > 0$, $\mu_H > 0$, and $\omega_H > 0$ be given. Define $V_{D_E}^0 := V_{D_E}/V_0$,

$$R_0 := \frac{V_0}{I_0}\frac{V_{D_E}^0\exp(\mu_H)}{V_{D_E}^0\cosh(V_{D_E}^0) - \sinh(V_{D_E}^0)}, \tag{50}$$

$$R_1 := \frac{V_0}{I_0}\frac{V_{D_E}^0\exp(\mu_H)}{\sinh(V_{D_E}^0)}, \tag{51}$$

and let α be a scalar parameter such that $\alpha > 1$. If the circuit parameters R, G_D, C_1, C_2, and L as chosen as

$$R \leq \frac{\alpha - 1}{2\alpha} R_0, \tag{52}$$

$$G_D = \frac{1}{R} + \frac{1}{R_1}, \tag{53}$$

$$C_1 = \frac{1}{\omega_H R_0} \sqrt{\frac{R_0}{R} - 1}, \tag{54}$$

$$C_2 = \frac{\alpha}{\omega_H R_0} \sqrt{\frac{R_0}{R} - 1}, \tag{55}$$

$$L = \frac{R_0}{\omega_H} \frac{1}{\left(\frac{R_0}{R} + \alpha\right) \sqrt{\frac{R_0}{R} - 1}}, \tag{56}$$

then the equilibrium point at $v_D = V_{D_E}$ of the Lur'e system (12)-(14) undergoes a supercritical Hopf bifurcation at $\mu = \mu_H$ generating a family of periodic solutions $v_D(t;\mu)$ for $\mu > \mu_H$ whose first-order approximations $v_D^0(t;\mu)$ in (41) are characterized by

$$A(\mu) = \bar{A}_0(\mu) V_0, \quad B(\mu) = \bar{B}_0(\mu) V_0, \quad \omega(\mu) = \omega_H, \tag{57}$$

where $\bar{A}_0(\mu)$ and $\bar{B}_0(\mu)$ are implicitly defined as the unique solution of the following equations

$$\begin{cases} \dfrac{A_0 \cosh(A_0)}{\sinh(A_0)} = \dfrac{B_0 \mathcal{J}_0(B_0)}{2\mathcal{J}_1(B_0)} \dfrac{V_{D_E}^0 \cosh(V_{D_E}^0)}{\sinh(V_{D_E}^0)} \\ \exp(\mu - \mu_H) = \dfrac{\sinh(A_0)}{A_0} \mathcal{J}_0(B_0) \dfrac{V_{D_E}^0}{\sinh\left(V_{D_E}^0\right)}. \end{cases} \tag{58}$$

Proof: See Appendix. ■

Remark 1: Note that $\alpha = C_2/C_1$, which means that C_1 should be chosen smaller than C_2, while (52) ensures that R is bounded above by $R_0/2$ for all $\alpha > 1$. It is interesting to observe that R_0 and R_1 depend on μ_H and V_{D_E}, while only C_1, C_2 and L depend also on ω_H. In particular, both R_0 and R_1 increase with μ_H and decrease with V_{D_E}. Also, from (50), (51), (52) and (72) in the proof of Proposition 1 it follows that the ratio Γ_H/R belongs to the interval $(1, 2)$. Since $\Gamma_H = \bar{L}(j\omega_H)$ and $R = \bar{L}(0)$, such a condition constrains the shape of the impedance of the linear part of the classic Chua's circuit (red box in Fig. 1).

Remark 2: In the proof of Proposition 1 it is shown that $\bar{A}_0(\mu)$ and $\bar{B}_0(\mu)$ are both increasing with μ. Hence, condition (42) is satisfied for all $\mu \in [\mu_H, \mu_{F_M}]$ where μ_{F_M} is such that

$$\bar{A}_0(\mu_{F_M}) + \bar{B}_0(\mu_{F_M}) = \frac{V_T}{V_0}. \tag{59}$$

From the second equation of (58) it follows that the width of the range $[\mu_H, \mu_{F_M}]$ is given by

$$\mu_{F_M} - \mu_H = \log\left(\frac{\sinh(A_0(\mu_{F_M})}{A_0(\mu_{F_M}} \mathcal{J}_0(B_0(\mu_{F_M}) \frac{V_{D_E}^0}{\sinh\left(V_{D_E}^0\right)} \right). \tag{60}$$

Since $\bar{A}_0(\mu_{F_M})$ and $\bar{B}_0(\mu_{F_M})$ are related by the first equation of (58) which is independent of μ_H, it follows that the width of $[\mu_H, \mu_{F_M}]$ depends only on V_{D_E}. In this respect, we observe that V_{D_E} is bounded above by V_T since $\bar{A}_0(\mu_H) = V_{D_E}^0$ and $\bar{B}_0(\mu_H) = 0$.

Proposition 1 ensures that for given $V_{D_E} > 0$, $\mu_H > 0$, and $\omega_H > 0$ there exists a unique PLCs family (41) whose bias $A(\mu)$, harmonic amplitude $B(\mu)$, and frequency $\omega(\mu)$ are given by (57). Moreover, this PLC family is generated by all the circuits with G_D, C_1, C_2, L as in (53), (54), (55), (56), respectively, and R and α belonging to the following region

$$\Lambda = \left\{ \alpha, R : \ \alpha > 1, \ \ R \leq \frac{\alpha - 1}{2\alpha} R_0 \right\}. \tag{61}$$

Such a degree of freedom in the circuit parameters can be exploited to choose suitable values on the basis of some practical aspects. Most importantly, it can be used to lower the distortion index (31) of the PLCs (41), thus making them better approximating the true limit cycles. Indeed, the distortion index (31) can be expressed as the following function of μ

$$D(\mu; \alpha, R) := D_1(\bar{A}_0(\mu) V_0, \bar{B}_0(\mu) V_0, \omega_H), \tag{62}$$

which depends on the values of α and R. Since $\bar{B}_0(\mu_H) = 0$ from (33) we have that $D(\mu; \alpha, R)$ vanishes at $\mu = \mu_H$, i.e., we have $D(\mu_H; \alpha, R) = 0$ for all $(\alpha, R) \in \Lambda$. According to Section II-D, one possible choice to select α and R is to make the distortion index at $\mu = \mu_F$ sufficiently small, i.e.

$$D(\mu_F; \alpha, R) \leq \varepsilon \tag{63}$$

where ε is some given positive constant.

Since the Hopf bifurcation is supercritical, the PLCs defined by (57) are stable at least when μ is close to μ_H. If a (supecritical) period-doubling bifurcation occurs at some larger value of μ then the PLCs are no longer stable. We can predict the occurrence of such a PPD bifurcation by exploiting condition (38) where (39) and (40) boil down to

$$F_0(A, B) = -\frac{I_0}{V_0} \exp(-\mu) \cosh\left(\frac{A}{V_0}\right) \mathcal{J}_0\left(\frac{B}{V_0}\right) \tag{64}$$

$$F_1(A, B) = -\frac{I_0}{V_0} \exp(-\mu) \sinh\left(\frac{A}{V_0}\right) \mathcal{J}_1\left(\frac{B}{V_0}\right). \tag{65}$$

Specifically, the PLCs family defined by (57) undergoes a (first) PPD bifurcation at $\mu = \mu_P$ if the following condition

$$\left| \bar{L}^{-1}\left(j\frac{\omega_H}{2}\right) - G_D - \frac{I_0}{V_0} \exp(-\mu) \cosh(A_0(\mu)) \ \mathcal{J}_0(B_0(\mu)) \right| - \frac{I_0}{V_0} \exp(-\mu) \sinh(A_0(\mu)) \ \mathcal{J}_1(B_0(\mu)) = 0, \tag{66}$$

holds for $\mu_P \in (\mu_H, \mu_F]$. Note that for fixed R, G_D, C_1, C_2, and L the PPD is detected as a zero of a scalar function of μ within the interval $[\mu_H, \mu_F]$.

Finally, the odd symmetry of the Lur'e system (12)-(14) implies that Proposition 1 applies also to the equilibium point

at $v_D = -V_{D_E}$, $V_{D_E} > 0$, with the unique difference that (57) becomes

$$A(\mu) = -\bar{A}_0(\mu)V_0, \quad B(\mu) = \bar{B}_0(\mu)V_0, \quad \omega(\mu) = \omega_H, \qquad (67)$$

where $\bar{A}_0(\mu)$ and $\bar{A}_0(\mu)$ are still the solutions of (58).

IV. DESIGN PROCEDURE AND APPLICATION EXAMPLES

In this section we first develop a procedure based on Proposition 1 to design the circuit parameters R, G_D, C_1, C_2, and L. Then, some application examples are discussed to illustrate the features of the procedure.

A. DESIGN PROCEDURE

The initial data of the procedure are the quantities characterizing the sought (supercritical) Hopf bifurcation, i.e., V_{D_E}, μ_H, ω_H, and the threshold V_T, which delimits the memristor voltage range where the gap remains practically constant over time. The procedure also involves the upper bound μ_F of the normalized gap interval and the quantity ε in the distortion index inequality (63). The values of these two parameters should be chosen in order that conditions (42) and (63) hold. Note that, according to Remark 2, (59) provides the upper bound μ_{F_M} of μ. Since $D(\mu; \alpha, R)$ vanishes at $\mu = \mu_H$, we have that there always exists μ_F satisfying (63) for any given value of ε.

The design procedure can be summarized in the following steps.

S1) Compute $\bar{A}_0(\mu)$ and $\bar{B}_0(\mu)$ solving the equations system (58).
S2) Compute the upper bound μ_{F_M} via (59) and pick any $\mu_F = \mu_F^0 \le \mu_{F_M}$.
S3) Compute the distortion index $D(\mu_F^0; \alpha, R)$ according to (31) and (62) and check if (63) is satisfied by some α and R belonging to the region Λ in (61) with G_D, C_1, C_2, L as in (53), (54), (55), (56), respectively.
S4) If so the design is completed and go to step S5); otherwise decrease μ_F^0 or increase ε and repeat step S3).
S5) Check via equation (66) if a PPD bifurcation occurs at $\mu = \mu_P$, $\mu_P \in (\mu_H, \mu_F^0]$.

Some comments on the procedure are in order. First, the structure of (58) greatly simplifies the computations in S1). Indeed, according to the proof of Proposition 1, the first equation admits a unique solution $A_0(B_0)$ for $B_0 \ge 0$, while the second one with A_0 replaced by $A_0(B_0)$ implicitly defines a unique function $B_0 = \bar{B}_0(\mu)$ for $\mu \ge \mu_H$, which in turn yields $\bar{A}_0(\mu) = A_0(B_0(\mu))$. Then, from (31) and (62) it follows that computing $D(\mu_F^0; \alpha, R)$ in S3) for a different value of μ_F^0 does not require to evaluate again the quantities $|L(jk\omega_H)|$. Finally, if for practical realization of the circuit we need to impose some bounds on the values of G_D, C_1, C_2, and L, they can be readily incorporated in the procedure. Indeed, these bounds simply define some sub-region Λ_S of Λ in (61) where the distortion index $D(\mu_F^0; \alpha, R)$ should be computed.

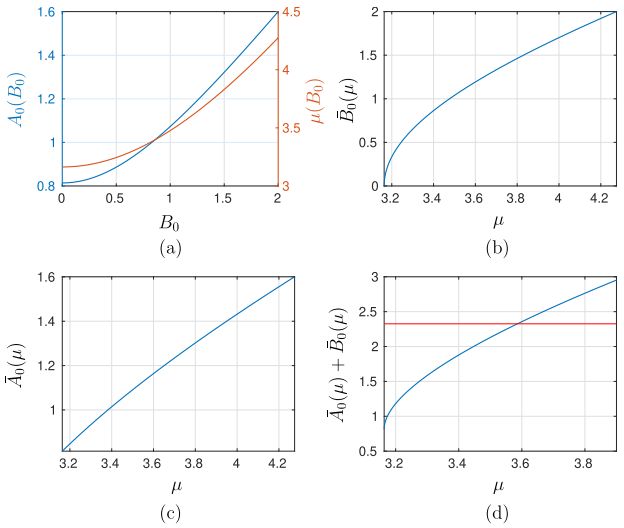

FIGURE 4. (a) $A_0(B_0)$ (blue curve) and $\mu(B_0)$ (red curve); (b) $\bar{B}_0(\mu)$; (c) $\bar{A}_0(\mu)$: (d) $\bar{A}_0(\mu) + \bar{B}_0(\mu)$ (blue curve) and V_T/V_0 (red curve).

The procedure provides the values of the circuit parameters G_D, R, C_1, C_2, and L ensuring that Proposition 1 holds and conditions (42) and (63) are satisfied. However, since the first-order HB method is approximate in nature, the PLCs (41) defined by (57) should be compared with the true periodic solutions $v_D(t; \mu)$ of the Lur'e system (12)-(14), i.e. system (7). To assess that the fulfillment of (4) ensuring that below threshold the dynamics of the gap g is indeed negligible, some comparison should be performed also with the dynamics displayed by the circuit of Fig. 1 once the memristor device is modeled via (1)-(3).

B. APPLICATION EXAMPLE

To illustrate the design procedure we consider the circuit studied in [19] where $V_{D_E} = 0.35\,V$, $\mu_H = 3.1636$, $\omega_H = 28.6\,krad/s$, and $V_T = 1\,V$. Also, we assume $\varepsilon = 0.02$, while μ_F is not fixed a-priori.

The solutions of the first equation of (58) are described by a unique function $A_0(B_0)$, while the second equation with $A_0 = A_0(B_0)$ defines the function $\mu(B_0)$. Both functions are reported in Fig. 4-(a). As expected, $\mu(B_0)$ is invertible and hence we get the sought functions $\bar{B}_0(\mu)$ and $\bar{A}_0(\mu) = A_0(B_0(\mu))$ of Fig.s 4-(b) and 4-(c), respectively. Note that both the functions are increasing with μ.

The upper bound of μ_F satisfying the constraint (59) is given by $\mu_{F_M} = 3.586$, as it can be verified from Fig. 4-(d) which displays $\bar{A}_0(\mu) + \bar{B}_0(\mu)$. We choose $\mu_F^0 = 3.5$ to ensure that (42) holds with some margin.

Since from (50) we get $R_0 = 702.5\,k\Omega$, the region Λ in (61) boils down to

$$\Lambda = \left\{\alpha, R:\ \alpha > 1,\ R \le \frac{\alpha - 1}{2\alpha}\, 702.5 \cdot 10^3\right\}$$

and it is depicted in Fig. 5. According to the practical considerations in [19] where the ratio $C_2/C_1 = \alpha = 10$ and

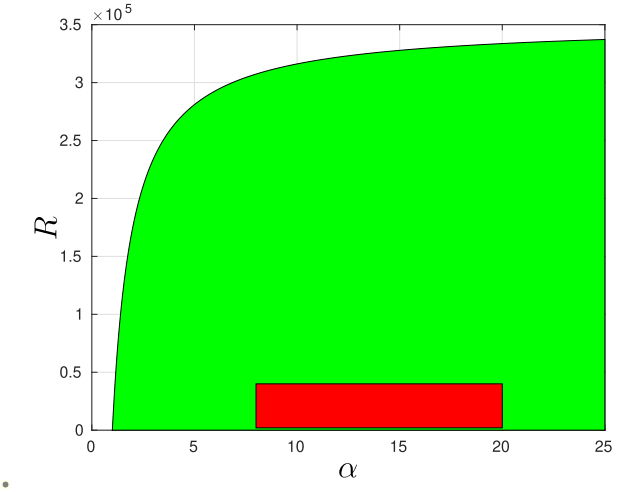

FIGURE 5. Regions Λ (green) and Λ_S (red).

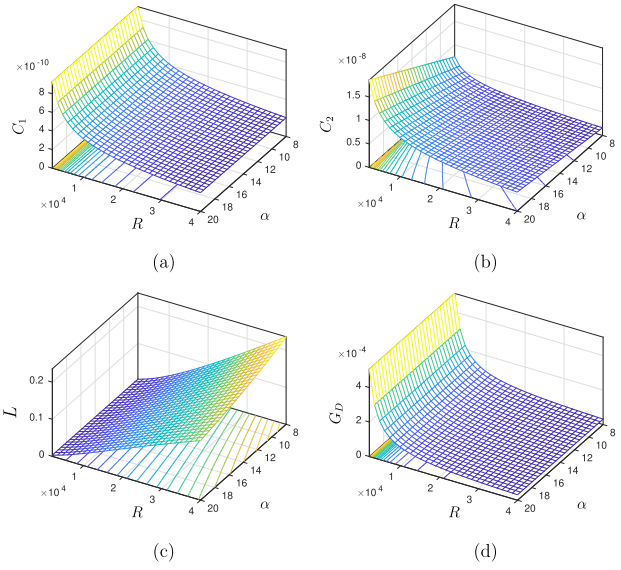

FIGURE 6. Circuit parameters for $(\alpha, R) \in \Lambda_S$: (a) C_1; (b) C_2; (c) L; (d) G_D.

$R = 32000$, we limit α and R to belong to the (red) rectangle in Fig. 5, i.e.

$$\Lambda_S = \{\alpha, R : \ \alpha \in [8, 20], \ R \in [2000, 40000] \}.$$

For each $(\alpha, R) \in \Lambda_S$ the values of C_1, C_2, L, and G_D are computed via (54), (55), (56), and (53), respectively. Figure 6 provides a graphical view of C_1, C_2, L, and G_D as a function of α and R. It is worth noting that C_1, C_2, and G_D decrease with respect to R, while L increases. Also, C_1, L, and G_D are almost constant with respect to α, while C_2 increases.

Then, we numerically compute the distortion index (62) at $\mu = \mu_F^0 = 3.5$ by using $K_h = 25$ harmonics terms in (31). Figure 7 reports the distortion index for $(\alpha, R) \in \Lambda_S$ together with its level curves. In particular, the level curves relative to $\varepsilon = 0.02$ and $\varepsilon = 0.012$ are highlighted in red and magenta, respectively.

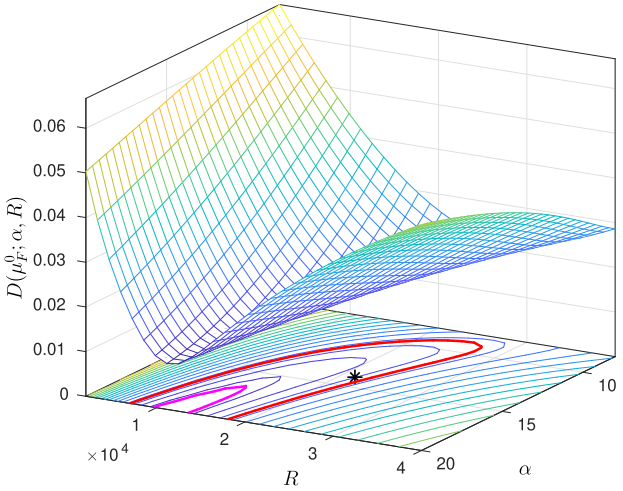

FIGURE 7. Distortion index $D(\mu_F^0; \alpha, R)$ for $(\alpha, R) \in \Lambda_S$, $\mu_F^0 = 3.5$. The red and magenta level curves correspond to $\varepsilon = 0.02$ and $\varepsilon = 0.012$, respectively. The selected values of R and α are marked by $\star$.

If we choose $\alpha = 14$ and $R = 21500\,\Omega$, we get $D(\mu_F^0; \alpha, R) = 0.020$ and the design procedure produces the following circuit parameters:

$$R = 21500\,\Omega, \ \ G_D = 5.3237 \cdot 10^{-5}\,\Omega^{-1},$$
$$C_1 = 0.28\,\mu F, \ \ C_2 = 3.92\,\mu F, \ \ L = 93.5\,mH. \qquad (68)$$

Finally, if for these values of R, G_D, C_1, C_2, and L we solve the scalar equation (66) with respect to μ, we get that a (first) PPD bifurcation is detected at $\mu = \mu_P = 3.2878$.

The circuit parameters (68) ensure that the Lur'e system (12)-(14) undergoes a supercritical Hopf bifurcation at $\mu = \mu_H = 3.1636$ generating a family of periodic solutions whose PLCs (41) are defined by (57) with $\bar{A}_0(\mu)$ and $\bar{B}_0(\mu)$ as in Fig. 4-(c) and Fig. 4-(b), respectively. Also, the PLCs are predicted to be stable until a (first) period doubling occurs at $\mu = \mu_P = 3.2878$. Since the PLCs are only approximations of the true periodic solutions, the dynamics of system (7) is investigated via numerical simulations using MATLAB. The peak-to-peak bifurcation diagrams are obtained integrating the differential equations (7) and (1)-(3) by means of the event-driven ODE15s routine. The results are summarized in Fig. 8 which reports the complete bifurcation diagram of the system[4] together with the first-order approximation given by $(\bar{A}_0(\mu) \pm \bar{B}_0(\mu))V_0$ (marked in red). It can be observed that the equilibrium point at the origin undergoes a pitchfork bifurcation at $\mu = 3.054$ with the birth of two stable symmetric equilibrium points which at $\mu = \mu_H$ are equal to $V_{D_E} = \pm 0.35\,V$ and undergo a supercritical Hopf bifurcation. For increasing values of μ the system displays a sequence of period doubling bifurcations leading first to a single-scroll attractors and then to double-scroll ones. The true and approximated periodic solutions display quite a similar behavior for $\mu \geq \mu_H$. Note that the generated true

[4]The diagram is quoted via the gap distance $g = \mu g_0$; the range corresponding to $[\mu_H, \mu_{F_M}]$ is $[0.87 \cdot 10^{-9}, 0.98 \cdot 10^{-9}]$.

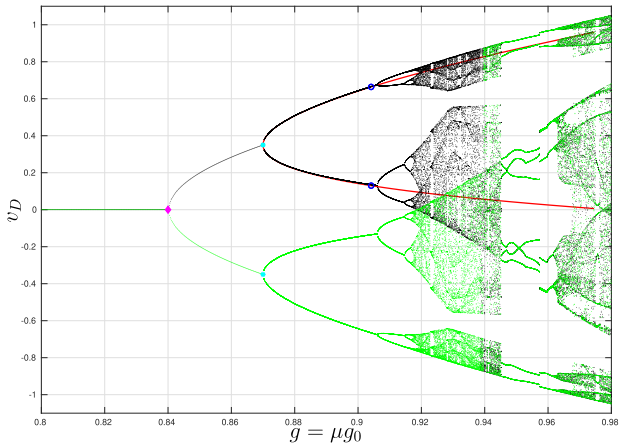

FIGURE 8. Bifurcation diagram of system (7) and the (first-order) approximation $(\bar{A}_0\ (g/g_0) \pm \bar{B}_0\ (g/g_0))V_0$ (red curve), when $V_{D_E} = 0.35\,V$. Magenta diamond and light blue disks denote pitchfork and Hopf bifurcations, respectively; blue circles denote predicted period-doubling bifurcations (PPDs).

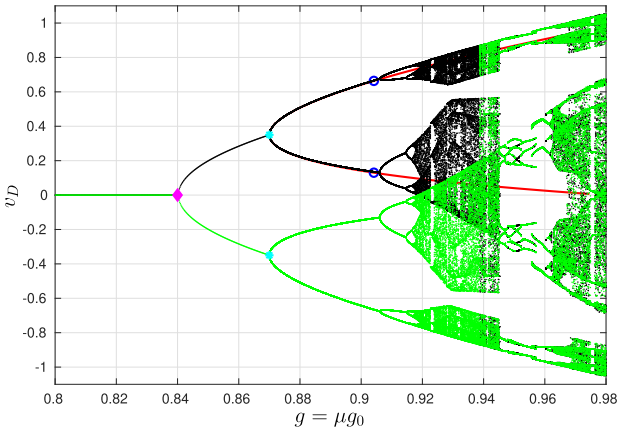

FIGURE 9. Bifurcation diagram of the circuit of Fig. 1 with the memristor device modeled via (1)-(3) and the (first-order) approximation $(\bar{A}_0\ (g/g_0) \pm \bar{B}_0\ (g/g_0))V_0$ (red curve), when $V_{D_E} = 0.35\,V$. Magenta diamond and light blue disks denote pitchfork and Hopf bifurcations, respectively; blue circles denote predicted period-doubling bifurcations (PPDs).

periodic solutions are stable until the system undergoes a first period-doubling bifurcation at $\mu = 3.294$, while the PPD is predicted to occur at $\mu_P = 3.2878$.

Finally, the dynamics of the circuit in Fig. 1 with the complete memristor model (1)-(3) and the circuit parameters as in (68) is analyzed via numerical simulations using MATLAB, obtaining the bifurcation diagram depicted in Fig. 9. As expected, its behavior is quite similar to that of Fig. 8 since in the range of the distance gap ($g \leq 0.98 \cdot 10^{-9}$ m) the threshold condition (59) is satisfied. It can be observed that the diagram still displays some odd symmetry, although the fifth-order system is no longer symmetric. Indeed, in the range of stable PLCs the system converges towards one of the two stable periodic solutions, depending on the initial conditions. As an example, Fig. 10 depicts the trajectories obtained by programming the normalized gap at $\mu = 3.273$.

C. DISCUSSION

In this section we provide some insights on how the design procedure depends on its initial data. First, we observe that ω_H influences only C_1, C_2, and L. Specifically, C_1, C_2, and L increase for decreasing values of the frequency of the solution generated by the Hopf bifurcation. As pointed out in Remark 1, all the circuit parameters depend on V_{D_E} and μ_H via either $V_T = 1$ V. Figure 11 reports R_0 and R_1 as function of $V_{D_E} \in [0, V_T]$, $V_T = 1$, for some fixed values of μ_H. It can be observed that both R_0 and R_1 increase with μ_H and decrease with V_{D_E}. This implies that the region Λ in (61) of the feasible values of R and α is larger for larger μ_H and smaller values of V_{D_E}.

According to (60) in Remark 2, the width of the range of μ, for which the voltage constraint (42) holds, depends only on V_{D_E}. Figure 12 shows that $\mu_{F_M} - \mu_H$ decreases with V_{D_E} and it equals zero when V_{D_E} reaches the threshold $V_T = 1$ V. Hence, choosing V_{D_E} much smaller than V_T guarantees larger

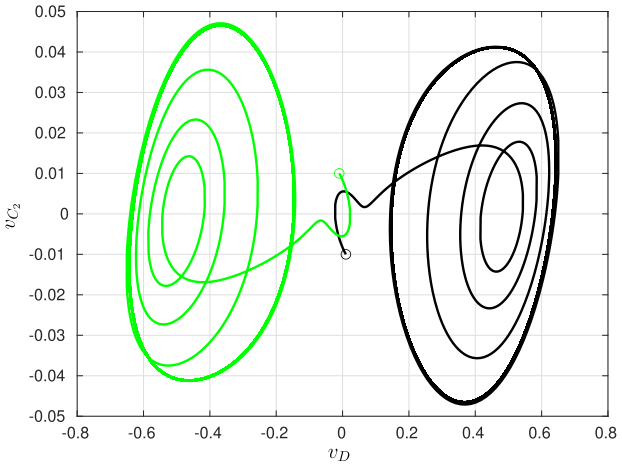

FIGURE 10. Trajectories on the $v_D - v_{C_2}$ plane of the circuit of Fig. 1 with the memristor device modeled via (1)-(3), starting from initial conditions $(v_D(0), v_{C_2}(0), i_L(0), g(0), T(0))$ equal to $(-0.01$ V, 0.01 V, $-1.4 \cdot 10^{-9}$ A, $0.9 \cdot 10^{-9}$ m, 278°K) (black) and (0.01 V, -0.01 V, $-1.4 \cdot 10^{-9}$ A, $0.9 \cdot 10^{-9}$ m, 278°K) (green), respectively. Circuit parameters have been chosen picking V_{D_E}, α and R as in the second row of Table 2; the normalized gap is programmed at $\mu = 3.273$.

ranges of μ where the third-order Lur'e system (12)-(14) and the fifth-order system with the complete memristor model (1)-(3) are expected to display similar dynamics.

Let us now consider the influence of V_{D_E} on the distortion index. To show this, we compute the values of μ_{F_M} corresponding to $V_{D_E} = 0.27$ V, $V_{D_E} = 0.35$ V, and $V_{D_E} = 0.5$ V (see Table 2). Then, we select $\mu_F^0 = 0.9\mu_{F_M}$ in all the three cases to compute the subregions of Λ_S where the distortion index satisfies $D(\mu_F^0; \alpha, R) \leq \varepsilon$ with $\varepsilon = 0.02$. Figure 13 reports the three subregions showing that the area increases with V_{D_E}. Hence, it is expected that the true periodic solutions of the Lur'e system are better approximated via the PLCs for larger values of V_{D_E}. A similar scenario is displayed also by the variation of the (first) PPD bifurcation with respect

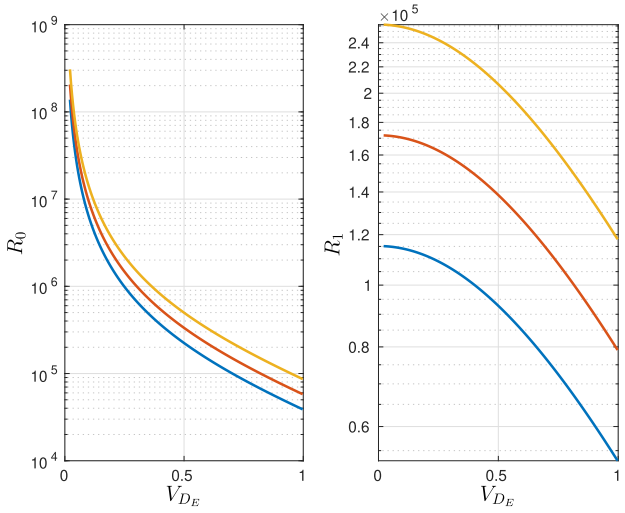

FIGURE 11. Behavior of R_0 (left) and R_1 (right) as functions of V_{D_E}, for $\mu_H = 2.8$ (blue), $\mu_H = 3.2$ (red) and $\mu_H = 3.6$ (orange).

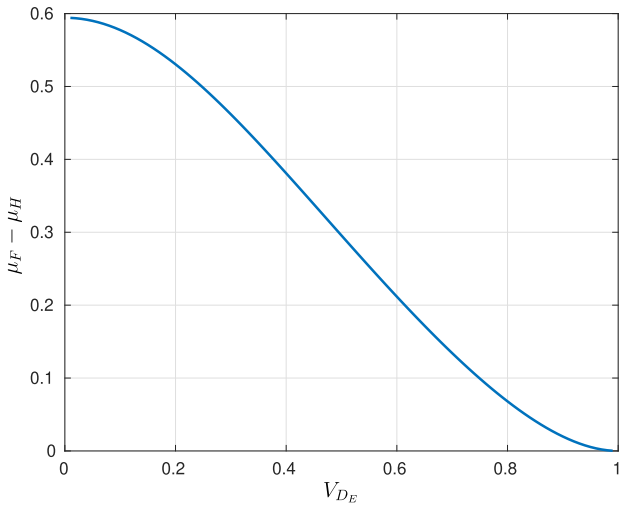

FIGURE 12. Behavior of $\mu_{F_M} - \mu_H$ as a function of V_{D_E}.

TABLE 2. Computation of μ_{F_M}, $D(\mu_F^0; \alpha, R)$, μ_P for the values of V_{D_E}, α and R chosen as in Figure 13.

V_{D_E}	μ_{F_M}	R	α	$D(\mu_F^0; \alpha, R)$	μ_P
0.27	3.648	20000	19.5	0.020	3.238
0.35	3.586	21500	14	0.020	3.288
0.5	3.459	20000	13	0.020	3.430

to V_{D_E}. To show this, we compute the values of μ_P for $V_{D_E} = 0.27$ V, $V_{D_E} = 0.35$ V, $V_{D_E} = 0.5$ V corresponding to the values of R and α marked in the corresponding subregions of Fig. 13. Table 2 shows that the predicted range $\mu_P - \mu_H$ of stable periodic solutions increases with V_{D_E}. This is confirmed by comparing the bifurcation diagram of Fig. 8 with those of Fig. 14 relative to $V_{D_E} = 0.27$ V and $V_{D_E} = 0.5$ V.

On the other hand, if we increase V_{D_E} it decreases the width $\mu_{F_M} - \mu_H$ of the range of μ where the voltage

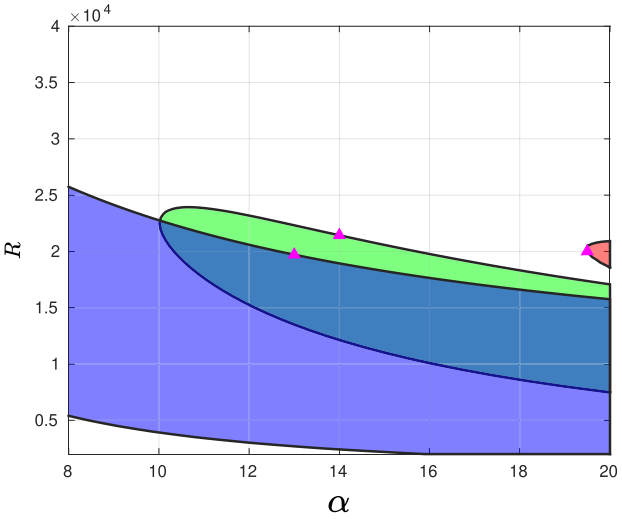

FIGURE 13. Subregions of Λ_S where the distortion index satisfies $D(\mu_F^0; \alpha, R) \leq \varepsilon$ with $\varepsilon = 0.02$, for $V_{D_E} = 0.27$ (red), $V_{D_E} = 0.35$ (green), and $V_{D_E} = 0.5$ (blue). The magenta triangles denote the points (α, R) reported in Table 2.

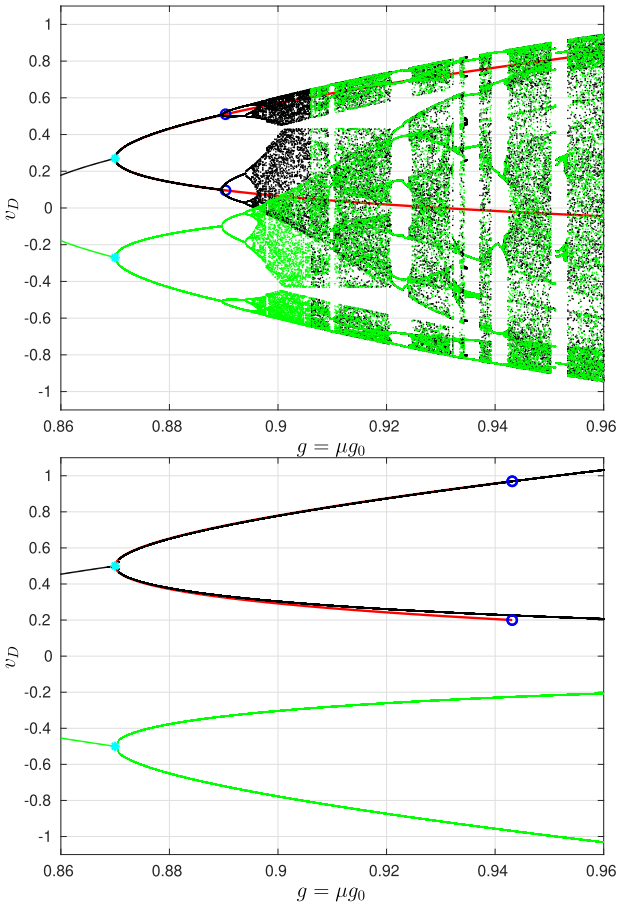

FIGURE 14. Bifurcation diagram of system (7) and the (first-order) approximation $(\bar{A}_0(\mu) \pm \bar{B}_0(\mu))V_0$ (red curve), when $V_{D_E} = 0.27\,V$ (top) and $V_{D_E} = 0.5\,V$ (bottom). Light blue disks denote Hopf bifurcations, respectively, blue circles denote predicted period-doubling bifurcations (PPDs).

constraint (42) holds. Hence, by increasing V_{D_E} it is expected that the dynamic behaviors of the third-order Lur'e system

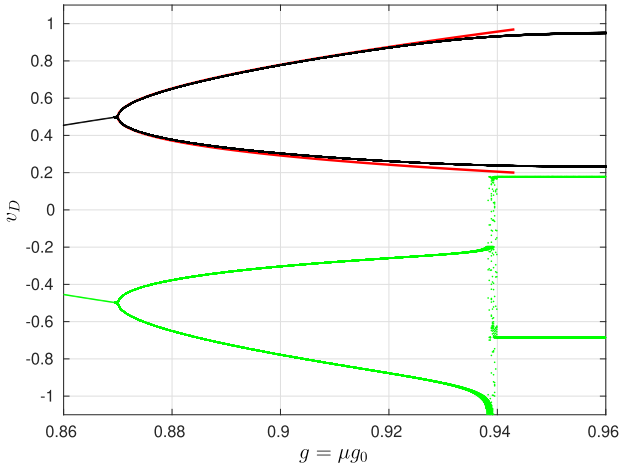

FIGURE 15. Bifurcation diagram of the circuit of Fig. 1 with the memristor device modeled via (1)-(3) and the (first-order) approximation ($\bar{A}_0(\mu) \pm \bar{B}_0(\mu)$)$V_0$ (red curve), when $V_{D_E} = 0.5\,V$.

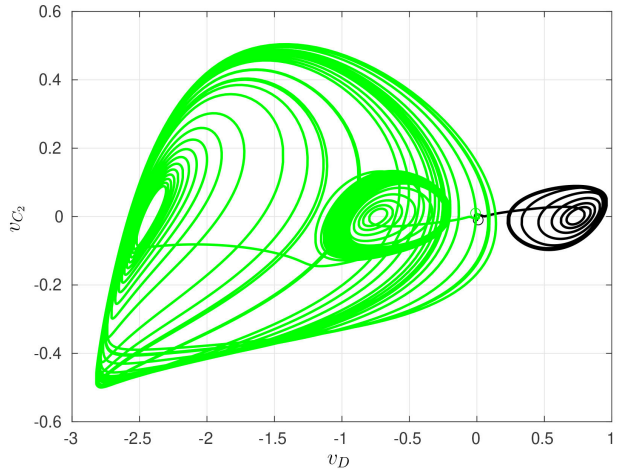

FIGURE 16. Trajectories on the $v_D - v_{C_2}$ plane of the circuit of Fig. 1 with the memristor device modeled via (1)-(3), starting from initial conditions ($v_D(0)$, $v_{C_2}(0)$, $i_L(0)$, $g(0)$, $T(0)$) equal to (-0.01 V, 0.01 V, $-1.4 \cdot 10^{-9}$ A, $0.94 \cdot 10^{-9}$ m, 278°K) (black) and (0.01 V, -0.01 V, $-1.4 \cdot 10^{-9}$ A, $0.94 \cdot 10^{-9}$ m, 278°K) (green), respectively. Circuit parameters have been chosen picking V_{D_E}, α and R as in the third row of Table 2; the normalized gap is programmed at $\mu = 3.418$.

(12)-(14) and the fifth-order system with the complete memristor model (1)-(3) can display significant differences. This is confirmed by comparing the bifurcation diagram of the fifth-order system pertaining to the case $V_{D_E} = 0.5$ V, which is reported in Fig. 15, with the one in Fig. 14 (top). It can be observed that, differently from the case $V_{D_E} = 0.35$ V (see Fig. 9 and Fig. 10), the diagram of Fig. 15 shows the presence of other dynamics even in the range of stable PLCs. Indeed, depending on the initial conditions the system can converge either to a periodic solution or to a single-scroll attractor, as shown in Fig. 16. This is due to the fact that the fifth-order system with the complete memristor model (1)-(3) is no longer symmetric when μ is close $\mu_{F_M} = 3.459$. Quite similar scenarios are obtained for larger value of V_{D_E}.

V. CONCLUSION

The paper has considered a circuit given by the interconnection of the linear part of classic Chua's circuit with a non-volatile memristor obeying the Stanford model, whose state variable, i.e., the gap distance, is known to display negligible time-variations when the voltage is below some threshold. A systematic procedure has been derived to ensure that some given equilibrium point of the circuit undergoes a supercritical Hopf bifurcation which generates stable periodic solutions within a given range of the gap distance. The procedure is based on: modeling the memristor as a programmable nonlinear resistor whose resistance depends on the gap distance which is assumed to be constant within the range; employing the first-order Harmonic Balance (HB) method to determine the set of the parameters giving rise to a supercritical Hopf bifurcation; selecting the parameters of the set ensuring that the Predicted Limit Cycles (PLCs) provided by the HB method are close to the stable periodic solutions generated by the Hopf bifurcation within the range of the gap. Although approximate in nature, the HB method accurately identifies Hopf bifurcations and thus the procedure permits to effectively design the parameters of the two-terminal element providing a family of stable periodic solutions which can be programmed by setting the value of the gap distance. This is illustrated via some application examples where also the sensitivity of the procedure with respect to the location of the equilibrium point and the range of the gap distance is discussed.

It is believed that the procedure can be suitably extended to cover the general case of circuits given by the interconnection of a linear time-invariant two-terminal (one port) element and a non-volatile memristor, under the assumption that the memristor can be modeled as a nonlinear programmable resistor within some voltage range.

APPENDIX
PROOF OF PROPOSITION 1

The proof proceeds by showing the following points: 1) the equilibrium point $v_D = V_{D_E}$ undergoes a Hopf bifurcation at $\mu = \mu_H$ for $\alpha > 1$, R satisfying (52), and G_D, C_1, C_2, L as in (53)-(56); 2) the first-order approximations $v_D^0(t;\mu)$ of the periodic solutions generated by the Hopf Bifurcation are characterized by (57)-(58); 2) the Hopf bifurcation is supercritical.

The first step of the proof is to show that for $\alpha > 1$, R satisfying (52), and G_D, C_1, C_2, L as in (53)-(56), the equilibrium point $v_D = V_{D_E}$ undergoes a Hopf bifurcation at $\mu = \mu_H$. Since $A_H = V_{D_E} > 0$ and $n(y) = i_D(y;\mu_H)$, condition (36) becomes

$$\begin{cases} V_{D_E} + L(0) I_0 \exp(-\mu_H) \sinh\left(\dfrac{V_{D_E}}{V_0}\right) = 0 \\ 1 + L(j\omega_H)\dfrac{I_0}{V_0} \exp(-\mu_H) \cosh\left(\dfrac{V_{D_E}}{V_0}\right) = 0. \end{cases} \tag{69}$$

Hence, taking into account (13), the Hopf bifurcution occurs at $\mu = \mu_H$ if and only if conditions (45) and (47) are satisfied

and we have

$$G_D - \frac{1}{R} - \frac{I_0}{V_0}\exp(-\mu_H)\frac{\sinh\left(V_{D_E}^0\right)}{V_{D_E}^0} = 0, \tag{70}$$

$$G_D - \frac{1}{\Gamma_H} - \frac{I_0}{V_0}\exp(-\mu_H)\cosh\left(V_{D_E}^0\right) = 0. \tag{71}$$

Note that, as expected, (70) and (71) are indeed the first-order HB equations (48) and (49) with $A_0 = V_{D_E}^0$, $\mu = \mu_H$, and $B = 0$, since $\lim_{B\to 0} J_0(B_0) = 1$ and $\lim_{B\to 0} J_1(B_0)/B_0 = 1/2$.

By substituting the expression (53) of G_D in the above equations we get that (70) is satisfied, while (71) holds if and only if

$$\frac{1}{\Gamma_H} = \frac{1}{R} - \frac{1}{R_0}. \tag{72}$$

Hence, according to (14), it remains to show that for $\alpha > 1$, R satisfying (52), and C_1, C_2, L as in (54)-(56) the following identity

$$\frac{\frac{1}{C_1}\left(\frac{1}{LC_2} - \omega_H^2 + j\omega_H\frac{1}{RC_2}\right)}{\frac{1}{RLC_1C_2} - \frac{1}{R}\left(\frac{1}{C_1}+\frac{1}{C_2}\right)\omega_H^2 + j\omega_H\left(\frac{1}{LC_2} - \omega_H^2\right)} = \frac{1}{\frac{1}{R} - \frac{1}{R_0}} \tag{73}$$

holds. It can be verified that (73) is indeed equivalent to the following two equations

$$\left(\frac{1}{LC_2} - \omega_H^2\right)^2 = \frac{1}{R^2C_2^2}\left(\frac{1}{LC_1} - \frac{C_2}{C_1} - 1\right)\omega_H^2, \tag{74}$$

$$\frac{\frac{1}{RC_1C_2}}{\frac{1}{LC_2} - \omega_H^2} = R_0\frac{1}{\left(\frac{R_0}{R} - 1\right)}. \tag{75}$$

Since from (54)-(56) we have $LC_1 = 1/(\omega_H^2(\alpha + R_0/R))$ and $C_2 = \alpha C_1$, it follows that (74) and (75) can be rewritten as

$$\frac{R_0^2}{\alpha^2R^2}\omega_H^4 = \frac{1}{R^2\alpha^2C_1^2}\left(\frac{R_0}{R} - 1\right)\omega_H^2 \tag{76}$$

and

$$\frac{\frac{1}{R\alpha C_1^2}}{\frac{R_0}{R\alpha}\omega_H^2} = R_0\frac{1}{\left(\frac{R_0}{R} - 1\right)}, \tag{77}$$

respectively, and thus they are both satisfied once C_1 is replaced with its expression in (54).

The second step of the proof is to show that the first-order approximations $v_D^0(t;\mu)$ of the periodic solutions generated by the Hopf bifurcation are given by (57)-(58). First, we observe that the first-order HB equations (48) and (49) admit solutions for $\mu \in [\mu_H, \mu_F]$ if and only if their right-hand sides are constant with respect to μ, which implies that

$$\frac{I_0}{V_0}\exp(-\mu_H)\frac{\sinh\left(V_{D_E}^0\right)}{V_{D_E}^0} = \frac{I_0}{V_0}\exp(-\mu)\frac{\sinh(A_0)}{A_0}\,\mathcal{J}_0(B_0) \tag{78}$$

and

$$\frac{I_0}{V_0}\exp(-\mu_H)\cosh\left(V_{D_E}^0\right) = \frac{I_0}{V_0}\exp(-\mu)\cosh(A_0)\;2\frac{\mathcal{J}_1(B_0)}{B_0}. \tag{79}$$

Since (79) can be replaced by the equation obtained by dividing term by term (78) and (79), i.e.

$$\frac{\sinh\left(V_{D_E}^0\right)}{V_{D_E}^0\cosh\left(V_{D_E}^0\right)} = \frac{\sinh(A_0)}{A_0\cosh(A_0)}\,\frac{B_0\mathcal{J}_0(B_0)}{2\mathcal{J}_1(B_0)}, \tag{80}$$

it follows that (78) and (80) are indeed equivalent to the first and second equation in (58), respectively. Hence, it remains to show that (58) admits a unique solution. To show this, we find it convenient to rewrite the first equation as

$$K(A_0) = K\left(V_{D_E}^0\right)\,H(B_0), \tag{81}$$

where

$$K(A_0) := \frac{A_0\cosh(A_0)}{\sinh(A_0)} \tag{82}$$

and

$$H(B_0) := \frac{B_0\mathcal{J}_0(B_0)}{2\mathcal{J}_1(B_0)}. \tag{83}$$

It can be verified that $K(0) = H(0) = 1$, $K'(A_0) > 0$ for $A_0 > 0$, $H'(B_0)$ for $B_0 > 0$, and $\lim_{A_0\to+\infty} K(A_0) = +\infty$, $\lim_{B_0\to+\infty} H(B_0) = +\infty$. Hence, it follows that (81) implicitly defines a unique smooth function $\bar{A}_0(B_0)$ such that $\bar{A}_0(0) = V_{D_E}^0$, $\bar{A}_0'(B_0) > 0$ for $B_0 > 0$, and $\lim_{B_0\to+\infty}\bar{A}_0(B_0) = +\infty$.

We observe that the second equation in (58) with $A_0 = \bar{A}_0(B_0)$ can be rewritten as

$$\mu = \mu_H + \log\left(\frac{\sinh(\bar{A}_0(B_0))}{\bar{A}_0(B_0)}\,\mathcal{J}_0(B_0)\frac{V_{D_E}^0}{\sinh\left(V_{D_E}^0\right)}\right), \tag{84}$$

which is indeed a function $\mu(B_0)$ for $B_0 \geq 0$. It can be readily verified that $\mu(0) = \mu_H$, $\mu'(B_0) > 0$ for $B_0 > 0$, and $\lim_{B_0\to+\infty}\mu(B_0) = +\infty$. This implies that (84) implicitly defines a function $\bar{B}_0(\mu)$ such that $\bar{B}_0(\mu_H) = 0$, $\bar{B}_0'(\mu) > 0$ for $\mu \geq \mu_H$, and $\lim_{\mu\to+\infty}\bar{B}_0(\mu) = +\infty$. Hence, we can conclude that $A_0(\mu) = \bar{A}_0(\bar{B}_0(\mu))$ and $B_0(\mu) = \bar{B}_0(\mu)$ provide the unique solution of (58).

The final step is to show that the Hopf bifurcation is supercritical by checking if the considered equilibrium point at $v_D = V_{D_E}$ becomes unstable for $\mu > \mu_H$ where it coexists with the generated periodic solution. According to (34) and

(35), the equilibrium point is given by the constant solution $\bar{v}_D(\mu)$, $\mu \geq \mu_H$, implicitly defined by the following equation

$$G_D - \frac{1}{R} = \frac{I_0}{V_0} \exp(-\mu) \frac{\sinh\left(\frac{\bar{v}_D(\mu)}{V_0}\right)}{\frac{\bar{v}_D(\mu)}{V_0}}. \tag{85}$$

Note that (70) implies $\bar{v}_D(\mu_H) = V_{D_E}$. Also, it can be verified that the constant solution $\bar{v}_D(\mu)$ is increasing for $\mu > \mu_H$. The stability properties of the equilibrium point defined by $\bar{v}_D(\mu)$ are characterized by the zeroes of $1+\bar{L}(s)i'_D(\bar{v}_D(\mu);\mu)$. Exploiting (13), (85), (70) and (71), it turns out that these zeroes are indeed those of the third order polynomial at the numerator of

$$1 + \bar{L}(s)\mathcal{K}(\bar{v}_D(\mu)), \tag{86}$$

where

$$\mathcal{K}(\bar{v}_D(\mu)) := \left(G_D - \frac{1}{R}\right)\left(K\left(\frac{\bar{v}_D(\mu)}{V_0}\right) - K\left(\frac{V_{D_E}}{V_0}\right)\right) - \frac{1}{\Gamma_H} \tag{87}$$

with $K(\cdot)$ is as in (82). Since $\mathcal{K}(\bar{v}_D(\mu_H)) = -1/\Gamma_H$, (45) and (47) imply that at $\mu = \mu_H$ there are two zeroes at $s = \pm j\omega_H$. The remaining zero is negative, since by factorizing the third order polynomial at the numerator of (86) as $(s^2 + \omega_H^2)(s + \sigma_0)$ we get $\sigma_0 = (1/R_0 + 1/(\alpha R))/C_1$. Since $\mathcal{K}(\bar{v}_D(\mu))$ is increasing for $\mu > \mu_H$, to complete the proof it is enough to show that for small $\theta > 0$ the third order polynomial at the numerator of $1+\bar{L}(s)(\theta - 1/\Gamma_H)$ has two zeroes with positive real part, while the third one remains negative by a continuity argument. Let $P(s;\theta) = s^3 + a_2(\theta)s^2 + a_1(\theta)s + a_0(\theta)$ denote such a polynomial whose coefficients depend on θ. It can be verified that

$$P(s;\theta) = \left(s + \left(\frac{1}{R_0} + \frac{1}{\alpha R}\right)\frac{1}{C_1}\right)(s^2 + \omega_H^2) + \frac{\theta}{C_1}\left(s^2 + \frac{1}{RC_2}s + \frac{1}{LC_2}\right), \tag{88}$$

and hence the coefficients $a_i(\theta)$, $i = 0, 1, 2$, are given by

$$a_2(\theta) = \frac{1}{C_1}\left(\frac{1}{R_0} + \frac{1}{\alpha R} + \theta\right),$$
$$a_1(\theta) = \omega_H^2 + \frac{\theta}{RC_1C_2},$$
$$a_0(\theta) = \frac{1}{C_1}\left(\omega_H^2\left(\frac{1}{R_0} + \frac{1}{\alpha R}\right) + \frac{\theta}{LC_2}\right).$$

Since $a_i(\theta) > 0$, $i = 0, 1, 2$, from the Routh-Hurwitz criterion it follows that $P(s;\theta)$ has two zeroes with positive real part for small $\theta > 0$ if and only if the following condition

$$a_2(\theta)a_1(\theta) - a_0(\theta) = \frac{\theta}{C_1}\left(\omega_H^2 + \left(\frac{1}{R_0} + \frac{1}{\alpha R}\right)\frac{1}{RC_1C_2} - \frac{1}{LC_2}\right) + \frac{\theta^2}{LC_1^2C_2} < 0$$

holds. Hence, it remains to show that we have

$$\omega_H^2 + \left(\frac{1}{R_0} + \frac{1}{\alpha R}\right)\frac{1}{RC_1C_2} - \frac{1}{LC_2} < 0. \tag{89}$$

Indeed, exploiting (54), (56) and taking into account that $C_2 = \alpha C_1$, condition (89) can be written equivalently as

$$\frac{\omega_H^2 R_0}{\alpha R}\frac{R - \frac{\alpha - 1}{2\alpha}R_0}{R_0 - R} < 0, \tag{90}$$

which is satisfied if and only if (52) holds, thus completing the proof.

REFERENCES

[1] M. M. Waldrop, "The chips are down for Moore's law," *Nature*, vol. 530, no. 7589, pp. 144–147, Feb. 2016.
[2] R. S. Williams, "What's next? [The end of Moore's law]," *Comput. Sci. Eng.*, vol. 19, no. 2, pp. 7–13, Mar. 2017.
[3] M. A. Zidan, J. P. Strachan, and W. D. Lu, "The future of electronics based on memristive systems," *Nature Electron.*, vol. 1, no. 1, pp. 22–29, Jan. 2018.
[4] L. Chua, "Resistance switching memories are memristors," *Appl. Phys. A, Solids Surf.*, vol. 102, no. 4, pp. 765–783, Mar. 2011.
[5] D. Ielmini and H.-S.-P. Wong, "In-memory computing with resistive switching devices," *Nature Electron.*, vol. 1, no. 6, pp. 333–343, Jun. 2018.
[6] O. Krestinskaya, A. P. James, and L. O. Chua, "Neuromemristive circuits for edge computing: A review," *IEEE Trans. Neural Netw. Learn. Syst.*, vol. 31, no. 1, pp. 4–23, Jan. 2020, doi: 10.1109/TNNLS.2019.2899262.
[7] C. Li, Z. Wang, M. Rao, D. Belkin, W. Song, H. Jiang, P. Yan, Y. Li, P. Lin, M. Hu, N. Ge, J. P. Strachan, M. Barnell, Q. Wu, R. S. Williams, J. J. Yang, and Q. Xia, "Long short-term memory networks in memristor crossbar arrays," *Nature Mach. Intell.*, vol. 1, no. 1, pp. 49–57, Jan. 2019.
[8] D. Ielmini and G. Pedretti, "Device and circuit architectures for in-memory computing," *Adv. Intell. Syst.*, vol. 2, no. 7, Jul. 2020, Art. no. 2000040.
[9] F. Corinto, M. Forti, and L. O. Chua, *Nonlinear Circuits and Systems With Memristors*. Cham, Switzerland: Springer, 2021.
[10] A. Ascoli, S. Slesazeck, H. Mähne, R. Tetzlaff, and T. Mikolajick, "Nonlinear dynamics of a locally-active memristor," *IEEE Trans. Circuits Syst. I, Reg. Papers*, vol. 62, no. 4, pp. 1165–1174, Apr. 2015.
[11] A. A. Sharma, Y. Li, M. Skowronski, J. A. Bain, and J. A. Weldon, "High-frequency TaO_x-based compact oscillators," *IEEE Trans. Electron Devices*, vol. 62, no. 11, pp. 3857–3862, Nov. 2015.
[12] J.-M. Ginoux, B. Muthuswamy, R. Meucci, S. Euzzor, A. Di Garbo, and K. Ganesan, "A physical memristor based Muthuswamy–Chua–Ginoux system," *Sci. Rep.*, vol. 10, no. 1, pp. 1–10, Nov. 2020.
[13] Y. Liang, G. Wang, G. Chen, Y. Dong, D. Yu, and H. H. Iu, "S-type locally active memristor-based periodic and chaotic oscillators," *IEEE Trans. Circuits Syst. I, Reg. Papers*, vol. 67, no. 12, pp. 5139–5152, Dec. 2020.
[14] S. Li, X. Liu, S. K. Nandi, S. K. Nath, and R. G. Elliman, "Origin of current-controlled negative differential resistance modes and the emergence of composite characteristics with high complexity," *Adv. Funct. Mater.*, vol. 29, no. 44, Nov. 2019, Art. no. 1905060.
[15] S. Kumar, J. P. Strachan, and R. S. Williams, "Chaotic dynamics in nanoscale NbO_2 Mott memristors for analogue computing," *Nature*, vol. 548, no. 7667, pp. 318–321, Aug. 2017.
[16] S. Kumar, R. S. Williams, and Z. Wang, "Third-order nanocircuit elements for neuromorphic engineering," *Nature*, vol. 585, no. 7826, pp. 518–523, Sep. 2020.
[17] Y. V. Pershin, S. N. Shevchenko, and F. Nori, "Memristive sisyphus circuit for clock signal generation," *Sci. Rep.*, vol. 6, no. 1, pp. 1–6, May 2016.
[18] L. Minati, L. V. Gambuzza, W. J. Thio, J. C. Sprott, and M. Frasca, "A chaotic circuit based on a physical memristor," *Chaos, Solitons Fractals*, vol. 138, Sep. 2020, Art. no. 109990.
[19] M. Di Marco, M. Forti, L. Pancioni, G. Innocenti, A. Tesi, and F. Corinto, "Oscillatory circuits with a real non-volatile Stanford memristor model," *IEEE Access*, vol. 10, pp. 13650–13662, 2022.

[20] M. Escudero, S. Spiga, M. Di Marco, M. Forti, G. Innocenti, A. Tesi, F. Corinto, and S. Brivio, "Chua's circuit with tunable nonlinearity based on a nonvolatile memristor: Design and realization," *IEEE Trans. Circuits Syst. I, Reg. Papers*, early access, Oct. 23, 2023, doi: 10.1109/TCSI.2023.3323854.
[21] M. Di Marco, M. Forti, G. Innocenti, and A. Tesi, "Harmonic balance method to analyze bifurcations in memristor oscillatory circuits," *Int. J. Circuit Theory Appl.*, vol. 46, no. 1, pp. 66–83, Jan. 2018.
[22] Q. Xu, Y. Lin, B. Bao, and M. Chen, "Multiple attractors in a non-ideal active voltage-controlled memristor based Chua's circuit," *Chaos, Solitons Fractals*, vol. 83, pp. 186–200, Feb. 2016.
[23] P. Sheridan, K.-H. Kim, S. Gaba, T. Chang, L. Chen, and W. Lu, "Device and SPICE modeling of RRAM devices," *Nanoscale*, vol. 3, no. 9, p. 3833, 2011.
[24] X. Guan, S. Yu, and H.-S. P. Wong, "A SPICE compact model of metal oxide resistive switching memory with variations," *IEEE Electron Device Lett.*, vol. 33, no. 10, pp. 1405–1407, Oct. 2012.
[25] Z. Jiang, S. Yu, Y. Wu, J. H. Engel, X. Guan, and H.-S. P. Wong, "Verilog—A compact model for oxide-based resistive random access memory (RRAM)," in *Proc. Int. Conf. Simul. Semiconductor Processes Devices (SISPAD)*, Sep. 2014, pp. 41–44.
[26] P.-Y. Chen and S. Yu, "Compact modeling of RRAM devices and its applications in 1T1R and 1S1R array design," *IEEE Trans. Electron Devices*, vol. 62, no. 12, pp. 4022–4028, Dec. 2015.
[27] H. K. Khalil, *Nonlinear Systems*. Upper Saddle River, NJ, USA: Prentice-Hall, 2002.
[28] A. I. Mees, *Dynamics of Feedback Systems*. New York, NY, USA: Wiley, 1981.
[29] D. P. Atherton, *Nonlinear Control Engineering*. London, U.K.: Van Nostrand Reinhold, 1975.
[30] A. Gelb and W. E. Vander Velde, *Multiple-Input Describing Functions and Nonlinear System Design*. New York, NY, USA: McGraw-Hill, 1968.
[31] M. Basso, R. Genesio, and A. Tesi, "A frequency method for predicting limit cycle bifurcations," *Nonlinear Dyn.*, vol. 13, pp. 339–360, 1997.
[32] G. Innocenti, A. Tesi, and R. Genesio, "Complex behavior analysis in quadratic jerk systems via frequency domain Hopf bifurcation," *Int. J. Bifurcation Chaos*, vol. 20, no. 3, pp. 657–667, Mar. 2010.
[33] A. Tesi, E. H. Abed, R. Genesio, and H. O. Wang, "Harmonic balance analysis of period-doubling bifurcations with implications for control of nonlinear dynamics," *Automatica*, vol. 32, no. 9, pp. 1255–1271, Sep. 1996.

MAURO DI MARCO received the Laurea degree in electronic engineering from the University of Firenze, Firenze, Italy, in 1997, and the Ph.D. degree from the University of Bologna, Bologna, Italy, in 2001.

From November 1999 to April 2000, he held a position as a Visiting Researcher with LAAS, Toulouse, France. Since 2000, he has been with the University of Siena, Siena, Italy, where he is currently an Associate Professor of circuit theory. He is the author of more than 100 international journals and conference papers. His current research interests include analysis and modeling of nonlinear dynamics of complex systems and neural networks, in robust estimation and filtering. From 2007 to 2011, he served as an Associate Editor for IEEE TRANSACTIONS ON CIRCUITS AND SYSTEMS—I: REGULAR PAPERS.

MAURO FORTI received the Laurea degree in electronics engineering from the University of Florence, Italy, in 1988.

From 1991 to 1998, he was an Assistant Professor of applied mathematics and network theory with the Electronic Engineering Department, University of Florence. In 1998, he joined the Department of Information Engineering and Mathematics, University of Siena, Italy, where he is currently a Professor of electrical engineering. His research interests include nonlinear circuits and systems, with emphasis on the qualitative analysis and stability of circuits modeling artificial neural networks. His research activity also includes aspects of electromagnetic compatibility.

Mr. Forti served as an Associate Editor for IEEE TRANSACTIONS ON CIRCUITS AND SYSTEMS—I: FUNDAMENTAL THEORY AND APPLICATIONS, from 2001 to 2003, and IEEE TRANSACTIONS ON NEURAL NETWORKS, from 2001 to 2010. He is serving as an Associate Editor for IEEE TRANSACTIONS ON CYBERNETICS, *Neural Networks*, and *Frontiers in Neuroscience*.

GIACOMO INNOCENTI received the master's degree in information engineering and the Ph.D. degree in nonlinear dynamics and complex systems from the University of Florence, in 2004 and 2008, respectively.

He was a Postdoctoral Research Fellow with the University of Florence and then with the University of Siena, from 2008 to 2010. Since 2012, he has been an Assistant Professor of automation with the University of Florence, where he is currently with the Department of Information Engineering. His research interests include nonlinear dynamics with particular interest in networks of interacting agents and neuron models. He serves as an associate editor for scientific journals in the field of the analysis of nonlinear systems and he was in the committees of workshops and scientific congresses on the same subject.

ALBERTO TESI received the Laurea degree in electronics engineering from the University of Florence, in 1984, and the Ph.D. degree in systems engineering from the University of Bologna, in 1989.

In 1990, he joined the Department of Systems and Computer Science, University of Florence, as a Research Assistant, where he is currently a Professor of control systems with the Department of Information Engineering. He is the coauthor of about 180 scientific publications. His research interests include analysis of nonlinear dynamics of complex systems, robust control of linear systems, and optimization.

Dr. Tesi was a member of the Conference Editorial Board of the Conference on Decision and Control, from 1994 to 1999, and the American Control Conference, from 1995 to 2000, and a member of the program committee of several international conferences. He was an Associate Editor of IEEE TRANSACTIONS ON CIRCUITS AND SYSTEMS, from 1994 to 1995, IEEE TRANSACTIONS ON AUTOMATIC CONTROL, from 1995 to 1998, and *Systems and Control Letters*, from 1995 to 2010.

Open Access funding provided by 'Università degli Studi di Siena' within the CRUI CARE Agreement